Thermal Stability and Surface Passivation of Ge Nanowires Coated by Epitaxial SiGe Shells

Shu Hu,[†] Yoko Kawamura,[‡] Kevin C. Y. Huang,[†] Yanying Li,[§] Ann F. Marshall,[⊥] Kohei M. Itoh,[‡] Mark L. Brongersma,[†,⊥] and Paul C. McIntyre*[,†,⊥]

[†]Department of Materials Science and Engineering, Stanford University, Stanford, California 94305, United States

[‡]School of Fundamental Science and Technology, Keio University, Yokohama, Japan; 3-14-1 Hiyoshi, Kohoku-ku, Yokohama 223-8522, Japan

[§]Department of Applied Physics, Stanford University, Stanford, California 94305, United States

[⊥]Geballe Laboratory for Advanced Materials, Stanford University, Stanford, California 94305, United States

S *Supporting Information*

ABSTRACT: Epitaxial growth of a highly strained, coherent SiGe alloy shell around a Ge nanowire core is investigated as a method to achieve surface passivation and carrier confinement, important in realizing nanowire devices. The high photoluminescence intensity observed from the core−shell nanowires with spectral features similar to that of bulk Ge indicates effective surface passivation. Thermal stability of these core−shell heterostructures has been systematically investigated, with a method demonstrated to avoid misfit strain relaxation during postgrowth annealing.

As-grown   Roughened   Smooth

KEYWORDS: *Core−shell nanowires, in situ transmission electron microscopy (TEM), thermal stability, photoluminescence*
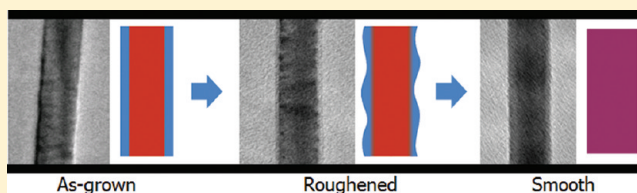
Germanium-silicon (group IV) core−shell nanowire (NW) heterostructures are promising building blocks to enable improved performance of nanophotonic and nanoelectronic devices. Bulk Ge has large intrinsic carrier mobilities, and Ge nanowires offer particularly interesting opportunities for on-chip light sources and detectors, as their absorption wavelengths can be matched to telecommunication standards.[1,2] However, surface passivation is an important requirement for realization of NW-based devices: Small diameter Ge nanowires have large surface area-to-volume ratio, and carrier scattering and recombination at surface defects may significantly compromise the electronic and optoelectronic properties of nanowire devices.

Heteroepitaxial growth of a Si or SiGe alloy shell around a Ge nanowire core has previously been explored to achieve surface passivation and carrier confinement, in part by promoting the formation of an outer Si/SiO_2 interface that can be passivated by hydrogen annealing[3] and by creating a core−shell band offset.[4−9] Either a pure Si shell or SiGe shell with high Si concentration allows for high quality, chemically stable SiO_2 surface oxide growth.[3,10] On the other hand, germanium oxides are water-soluble and have poor thermal stability, hindering their use as an insulating surface passivation layer.[11] For suitable choices of materials and dimensions, a large band offset in a heteroepitaxial passivated Ge nanowire may also confine the carriers to the Ge core, away from surface states, and thus increase the effective conductance. Band offsets also allow for modulation doping, where ionized dopants incorporated in the shell can provide free carriers to an intrinsic

core that is spatially separated from dopant scattering centers. In nanophotonic devices, confining carriers away from the surface can increase the emission efficiency, by maintaining radiative electron−hole recombination.

To achieve the desired structural characteristics for heteroepitaxial surface passivation of Ge nanowires with a large core−shell band offset, conformal deposition of a thin SiGe shell with high Si concentration is required. The resulting core−shell misfit strain is large; however, nanoscale objects are more elastically compliant than bulk solids and thin films constrained by bulk substrates. The cylindrical geometry of core−shell nanowires can accommodate larger misfit strain than is possible in planar thin film structures.[12] Moreover, the maximum misfit strain possible in core−shell nanowires increases with increasing shell thickness beyond a certain thickness value, contrary to the situation for planar thin films on bulk substrates. Two strategies for growth of initially coherent misfitting SiGe shells on Ge core nanowires have been reported previously:[9] (1) HCl flow to inhibit surface roughening during the Si or SiGe shell growth and (2) epitaxial growth of Si shells on low-energy sidewall facets that resist surface roughening. Another way to realize core−shell heterostructures in this system is to deposit amorphous Si shells at low temperatures and subsequently recrystallize the shells seeded by the crystalline cores.[13]
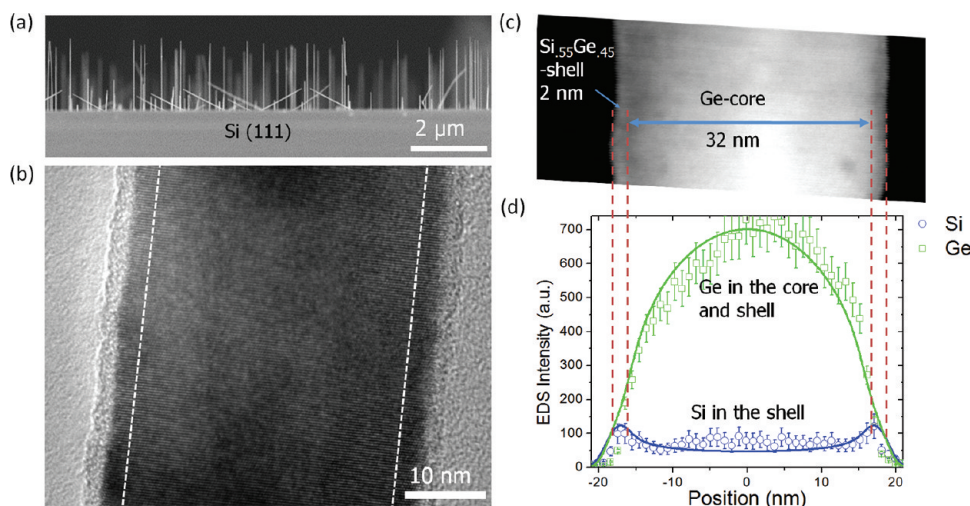
Figure 1. Structural and chemical composition analysis of highly strained coherent Ge-core/SiGe-shell nanowires. (a) SEM image of the as-grown core−shell nanowires on a Si (111) substrate. (b) High-resolution TEM image of a dislocation-free 32 nm Ge-core/2 nm $Si_{0.55}Ge_{0.45}$-shell nanowire. The dashed lines indicate the estimated position of the core−shell interfaces. (c) Dark-field scanning TEM image and (d) Si and Ge EDS line profiles of the core−shell nanowire in (b). The continuous curves are the fitted Si and Ge EDS intensity profiles. The nanowire was aligned parallel to the $[\bar{1}10]$ zone axis as shown in panels b and c.

Many postgrowth device fabrication steps exist after the growth of highly strained, initially coherent nanowire heterostructures. Some of these involve thermal annealing at elevated temperatures. For typical nanoelectronic devices, postgrowth thermal processes include annealing,[4,6,14] dopant implantation, and dopant activation.[4] For example, thermal oxidation to form high quality Si/SiO_2 interfaces with low interface defect densities usually requires temperatures above 800 °C.[10]

Postgrowth thermal processing can produce morphological changes and strain relaxation in the initially coherent core−shell nanowires. This may cause the nanowire core to lose the surface passivation and engineered strain. To optimize nanowire device performance, it is of vital importance to understand how postgrowth thermal processes affect surface morphology, coherency strain, and chemical composition of core−shell heterostructures. Here, we report on the effects of postgrowth thermal processing on the coherency strains, radial composition distribution, and surface roughness of highly strained Ge/SiGe core−shell nanowires. Use of intentional surface oxidation to suppress roughening and loss of interface coherency is also discussed. In addition, strong band-edge photoluminescence, comparable to that of bulk Ge, is observed from the SiGe shell-passivated VLS-grown Ge NWs.

Epitaxial growth of a 2 nm SiGe shell with ∼55% Si concentration around a ⟨111⟩-oriented Ge nanowire core was achieved, producing highly strained, dislocation-free, core−shell nanowires by inhibiting surface roughening during shell growth. Au-catalyzed, chemical vapor deposited Ge nanowires were first synthesized, followed by heteroepitaxial deposition of a SiGe shell. Vertically aligned Ge nanowire cores were grown from colloidal Au nanoparticles randomly dispersed on a Si (111) substrate using an initial nucleation step at 375 °C followed by steady-state growth to a length of ∼2 μm at 300 °C.[15] The Au catalyst nanoparticle at the tip of the Ge nanowire was not removed prior to the shell deposition. Catalyzed axial growth through the Au nanoparticles resulted in a small segment of SiGe alloy nanowires between the Au tip and core−shell nanowire. An SEM cross-sectional image (Figure 1a) shows

arrays of as-grown core−shell nanowires on a Si (111) substrate.

Si and Ge composition line profiles across the core−shell nanowire diameter were analyzed using transmission electron microscopy (TEM) with energy-dispersive X-ray spectroscopy (EDS). The characterization was performed using an FEI Tecnai G2 F20 TEM operating at 200 kV. The as-grown core−shell nanowire in Figure 1 exhibits a 32 nm Ge-core/2 nm $Si_{0.55}Ge_{0.45}$-shell geometry. Two methods were used to determine the Si atomic composition x in the Si_xGe_{1-x} shell and the shell thickness t_s. When the nanowire is aligned "edge-on", the electron beam can directly probe the shell composition by passing through the shell only. This can be extracted from the shell portion of the Si and Ge EDS line profiles that scale linearly with the beam position. The dark-field scanning TEM image in Figure 1c clearly shows the Ge core and the SiGe shell, as indicated by the brighter contrast Ge-rich region at higher atomic number and the lighter contrast SiGe shell at lower atomic number. ∼32 nm Ge-core and 2 nm SiGe-shell was measured directly. In addition, a model considering the thickness and composition of a cylindrical core and a uniform shell is used to simulate and fit both the core−shell geometry and shell composition, similar to the method reported by Varahramyan et al.[8] We assume the X-ray absorption in the electron beam path is negligible because of the very small thickness of the nanowires. The fitted curves for the Si and Ge intensity profiles are shown as the continuous plot in Figure 1d. The slight discrepancy at the center position is due to the faceted cross section of as-grown nanowires, different from the circular one in the simplified model used to analyze the EDS data. The fitted core diameter d_c is 32 ± 1 nm, and the Si_xGe_{1-x}-shell thickness t_s is 2 ± 1 nm with a Si atomic composition $x = 55 \pm 5\%$ in the shell.

Photoluminescence (PL) is a powerful tool for assessing the structural quality of epitaxial heterostructures[16,17] because detection of band-edge PL generally requires a low density of surface and interface recombination centers. This technique is often used to probe for the presence of surface and interface states[18,19] and misfit dislocations[20,21] in planar heteroepitaxial
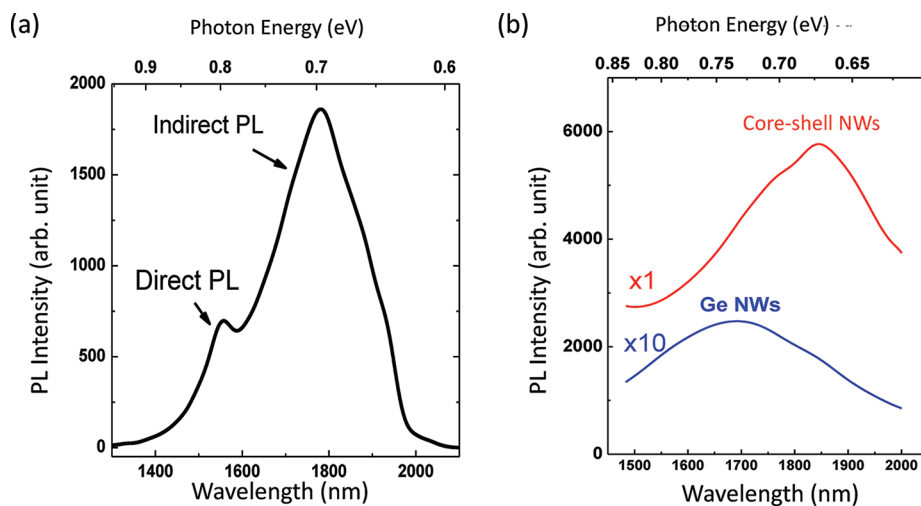
Figure 2. Photoluminescence spectra acquired with 40 mW laser excitation and a 10× microscope objective: (a) PL from a Ge (111) substrate; (b) PL from 40 nm Ge-core/2 nm $Si_{0.55}Ge_{0.45}$ shell NWs grown on a Si (111) substrate and from 40 nm diameter Ge NWs.

structures such as semiconductor quantum wells. The number of PL studies involving Ge NWs is limited because it is usually difficult to detect significant emission intensity. It has been reported previously that carrier trapping at unpassivated surface states and subsequent nonradiative recombination typically dominate carrier relaxation in semiconductor nanowires.[22,23] The unpassivated surface states of Ge NWs provide a high density of nonradiative recombination centers, and this is the likely cause of strongly attenuated PL intensities for band-to-band transitions. Kamenev et al. have investigated PL from free-standing Ge NWs grown on Si substrates in the near-infrared (NIR) wavelength region.[24] However, the Ge NWs did not exhibit detectable PL intensities near the Ge band gap.

Photoluminescence spectroscopy was employed to assess the quality of the initially coherent core−shell surface passivation, particularly in a 40 nm Ge-core/2 nm $Si_{0.55}Ge_{0.45}$-shell geometry. PL spectra from arrays of 40 nm Ge-core/2 nm $Si_{0.55}Ge_{0.45}$-shell nanowires and bulk Ge (111) substrates (p-type Ga dopant, resistivity of 1.8−2.3 ohm·cm) were compared. Both samples were pumped with a continuous-wave Nd:YAG laser source at a wavelength of 532 nm. The high PL intensity observed from the core−shell nanowire arrays and the same emission behavior as compared to the bulk Ge substrate suggest good surface passivation of Ge nanowire cores. Figure 2 displays the NIR room-temperature PL spectra of the core−shell nanowire arrays measured with 40 mW laser excitation and a 10× microscope objective. For comparison, PL from bulk Ge (111) single crystal substrates was measured under the same excitation conditions. As shown in Figure 2a, two PL peaks appear in the wavelength range of 1500−2000 nm, corresponding to Ge indirect- and direct-band gap radiative recombination at the indirect band gap of 0.70 eV (1.77 μm) and direct band gap of 0.80 eV (1.55 μm). Both the indirect-band gap and direct-band gap PL peak positions are consistent with previous reports for bulk samples.[25−27] As shown in Figure 2b, the measured peak intensity for core−shell nanowires was higher than that for the bulk Ge substrate and was 10× higher than that for the bare Ge NWs without a crystalline SiGe shell. The photoluminescence via transitions across the direct band gap of Ge that is observed for the bare Ge NWs will be discussed in more detail in an upcoming publication.[28] The PL peak positions for both the bare Ge NWs and the core−shell NW

arrays are comparable to the direct and indirect PL peak positions for the bulk Ge, respectively, with a small red shift for both peaks consistent with the effect of laser heating of the nanowires.[28] This is, to our knowledge, the first reported experimental observation of band-edge photoluminescence from group IV core−shell nanowire heterostructures. The fact that it is observed from NW arrays with Au catalysts still present indicates that nonradiative carrier recombination at any residual Au impurity atoms is insufficient to quench the strong photoluminescence from these passivated nanostructures.

The 20−40 nm Ge core/2 nm $Si_{0.55}Ge_{0.45}$-shell nanowires, though apparently dislocation-free and coherent as-grown, have a greater tendency to relax their misfit strains during postgrowth thermal processes. According to EDS/STEM chemical analysis, the Si concentration profile along the radius direction is close to a step function: the Si atomic composition is ∼55% in the SiGe shell and almost immediately drops to 0% in the Ge core. This composition drop corresponds to a ∼2.3% core−shell lattice mismatch. Furthermore, such a core−shell heterostructure is in a metastable state for forming interfacial defects, such as misfit dislocations. Liang et al. modeled the stress and strain in a cylindrical shape core−shell wire with a coherently strained heteroepitaxial interface.[29] For a 32 nm core with a 2 nm shell, the equilibrium misfit strain is 1.1%. The as-grown nanowires we have investigated are predicted to have a 2.3% misfit strain, more than twice the thermodynamic limit. When a $Si_{0.55}Ge_{0.45}$ shell thicker than 2 nm is deposited on a ∼40 nm Ge nanowire, the shell became roughened and dislocations were observed prior to any annealing. For 20 nm diameter Ge NW cores, only surface roughening was observed, presumably because thinner Ge cores were more elastically compliant.[12] Additional images and discussion of this point are included in the Supporting Information.

Strain relaxation mechanisms of Ge/SiGe core−shell heterostructures, including Si−Ge interdiffusion, stress-driven surface roughening, and associated dislocation formation, were investigated. For initially strained two-dimensional hetero-epitaxial thin films, Si−Ge interdiffusion[30−33] has been investigated extensively. In core−shell nanowires, the Si and Ge atoms may interdiffuse radially, driven by the composition gradient and misfit strain elastic energy. Other strain relaxation processes for heteroepitaxial thin films on planar bulk substrates
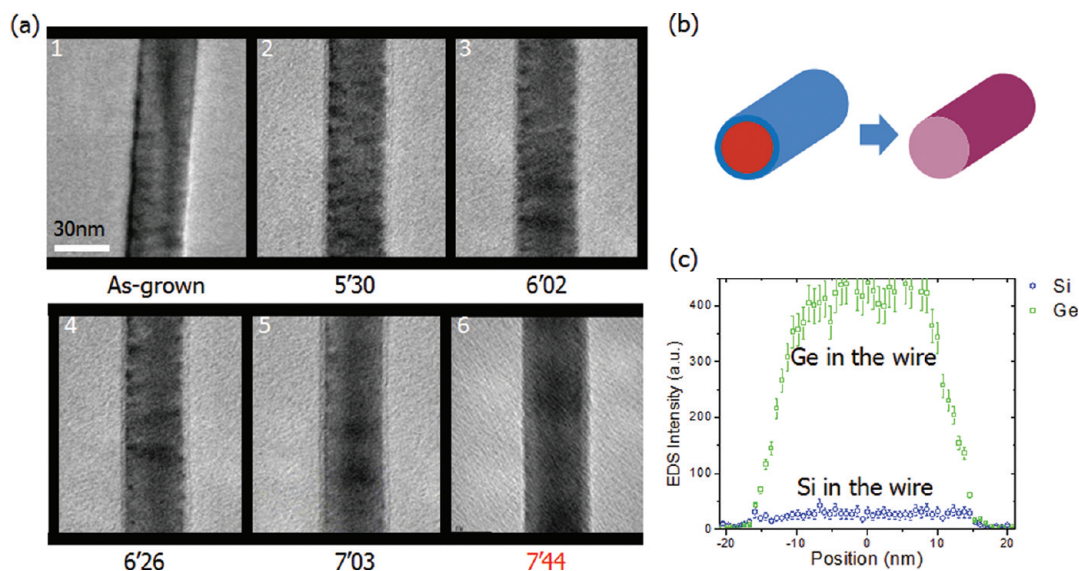
Figure 3. In situ thermal stability study of initially coherent core–shell nanowires in TEM. (a) Frames from the video recorded before and during annealing at 700 °C in vacuum in the TEM column. (b) Schematic illustration of Si–Ge interdiffusion in a cylindrical core–shell nanowire heterostructure. (c) Si and Ge EDS signal intensities for Si and Ge chemical composition analysis of the same nanowire in (a), after annealing at 700 °C for 20 min in vacuum.

include stress-driven surface roughening and dislocation formation, where surface roughening proceeds and promotes dislocation nucleation.[34−36] In core–shell nanowires, similar processes during annealing may exist as well. During annealing, the core–shell misfit strain drives a diffusional atomic flux along the surface in a way that the initially atomically smooth sidewall evolves into an undulating profile with hill-and-valley structure.[12,37] When the SiGe shell breaks up in this manner, some relief of the axial tensile strain of the Si shell is achieved at the peaks, and thus there is an energetic driving force for adatoms to diffuse from the valleys to the peaks. Schmidt et al.[37] performed a stability analysis of the roughening of such misfit-strained cylindrical core–shell nanowires. Roughening of the surface promotes dislocation nucleation due to the high stress concentrated at the valleys of the surface undulation.[34]

The thermal stability of highly strained as-grown core–shell nanowires was first investigated by heating in the TEM column. As-grown 32 nm Ge-core/2 nm $Si_{0.55}Ge_{0.45}$ shell nanowires with 2.3% misfit strain were annealed in the TEM at 700 °C for 20 min in vacuum. Figure 3a shows frames from a video recorded at various stages of in situ annealing. Note that the gray background surrounding the crystalline nanowire is the supporting holey carbon film of the TEM grid. Within 8′47 min of annealing at 700 °C, the initially coherent core–shell nanowire surfaces roughen and then become smoother again. Frame 2 is a video frame immediately before the onset of roughening of the shell surface, corresponding to 5′30 min annealing at 700 °C. Surface roughening was observed simultaneously on all the sidewall facets of the core–shell nanowires sampled in this experiment. Within the next minute, the sidewall facets became increasingly rough as shown in frames 3 and 4. While the amplitude of the undulation on the roughened surface increases over time, the periodicity remains the same. The measured periodicity of 8.3 ± 0.4 nm corresponds to the fastest growth mode, that is, asymmetric hills and valleys on the opposite sides of sidewall facets. This may be determined by the core–shell geometry and misfit strain.[37] The surface roughness reached a maximum peak-to-

peak value of 1.8 ± 0.1 nm at 6′26 min of annealing. Both the amplitude and periodicity of observed undulation on the roughened surface started to decrease with time, as shown in frames 5 and 6. After ~8 min of annealing, the nanowire surface became similarly smooth compared to its initial state. It is interesting to notice that this dynamic roughening and smoothing behavior is not normally observed in planar thin film heterostructures.[38] For planar thin films, smoothing is expected when misfit strain between two homogeneous films is reduced through formation of interfacial defects[39] or when elastic strain energy is decreased due to lateral phase separation within thin films.[40]

Si–Ge interdiffusion was found to be the primary strain relaxation mechanism at 700 °C for core–shell nanowires with 2.3% core–shell strain. Figure 3b illustrates the occurrence of significant interdiffusion in the bulk, showing a uniform Si composition profile after the TEM anneal, without distinguishable core/shell interface. The Si and Ge EDS signal intensities in Figure 3c increase and decrease as the electron-beam probe scans across the wire diameter, and they scale only with the approximate wire thickness through which the electron beam passes. The observed rough-to-smooth surface transition is consistent with decreasing core–shell misfit strain during the 700 °C annealing. Qualitatively, once the elastic strain driving force for roughening is consumed by Si–Ge interdiffusion, capillary effects should cause the wire surface to smooth out again. It is possible that dislocations nucleated as a result of the observed surface roughening in frames 2–4 (Figure 3a) and then annihilated after significant Si–Ge interdiffusion.

The experimental results can be compared to model predictions to determine the mechanism by which strain is relaxed. Without considering core–shell misfit strain, the Si–Ge interdiffusivity can be described by the following semi-empirical equation, using experimentally measured values for Si–Ge interdiffusion in relaxed SiGe films of high Ge content (average Ge composition of 91 at. %):[30] $\tilde{D}(T) = 3.6 \exp(-3.20$ eV$/kT)$ cm^2/s, where k is the Boltzmann constant and T is the temperature. At 700 °C, the interdiffusivity $\tilde{D}_{700°C} \approx 9.6 \times$
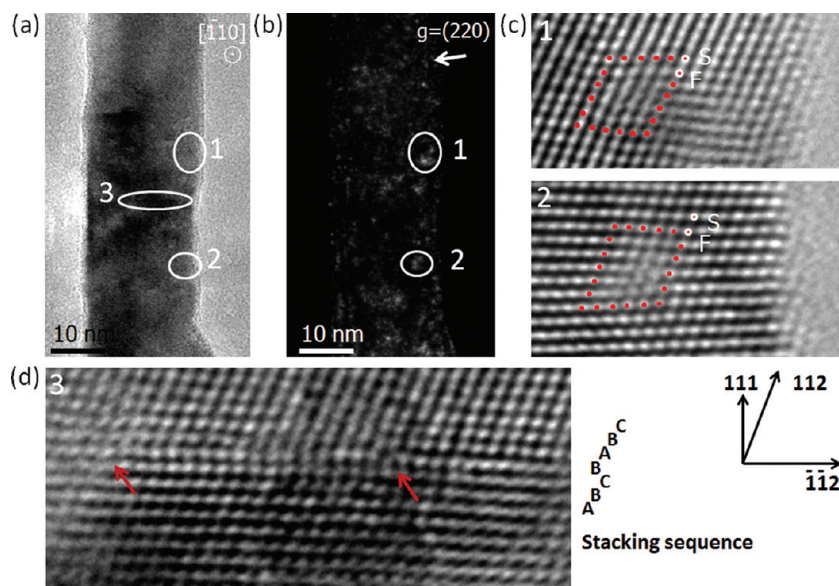
Figure 4. TEM images of a 20 nm Ge-core/2 nm $Si_{0.55}Ge_{0.45}$-shell nanowire after annealed in hydrogen at 600 °C for 6 min. (a) Bright-field image taken with the nanowire aligned on a [$\bar{1}$10] zone axis. (b) Weak-beam dark-field (WBDF) image with a (220) reflection. (c) High-resolution images of ⟨110⟩-type perfect dislocations around which the Burgers vector loop is drawn. (d) High-resolution image of an intrinsic stacking fault bounded by two Shockley partial dislocations, as indicated by two red arrows.

10^{-17} cm²/s. The relatively high Si−Ge interdiffusivity for this temperature results from the high average Ge composition of the core−shell nanowires. For 8 min annealing, the characteristic interdiffusion length $(\tilde{D}_{700°C}t)^{1/2}$ is about 2.1 nm, close to a shell thickness of 2 nm. Furthermore, diffusion by a vacancy mechanism in biaxially strained SiGe films is found to be enhanced by increased vacancy concentration compared to equilibrium vacancy concentration in relaxed films.[41] It is generally accepted that both Si tracer diffusion in Ge and Si diffusion in high Ge concentration films occur primarily by a vacancy mechanism.[42] Therefore, the Si−Ge interdiffusivity will be enhanced by the axial tensile strain in a strained SiGe shell. Under tensile strain, the estimated characteristic Si−Ge interdiffusion length for 8 min annealing could be significantly larger than the measured shell thickness.

For core−shell nanowires after annealing in the TEM at 550 °C in vacuum for ∼11 min, slightly roughened surfaces were observed and further annealing did not smooth them out. Compared to the 700 °C anneals, surface roughening mediated by stress-driven surface diffusion is less pronounced. At 550 °C, the Si−Ge interdiffusion kinetics are suppressed: the characteristic interdiffusion length is predicted to be ∼0.07 nm, much less than the shell thickness.

In situ annealing in the TEM at 700 °C was also performed for smaller-diameter Ge cores, e.g., 20 nm Ge-core/2 nm $Si_{0.55}Ge_{0.45}$ shell nanowires (shell deposited under the same conditions as the samples in Figure 1). Similar to the 32 nm diameter core specimens, the initially coherent core−shell interface evolves from slightly undulating to rough to smooth again. Roughened sidewall surfaces were detectable after 6′18 min annealing and disappeared after ∼9 min annealing. STEM-EDS analysis once again confirms the strain relaxation mechanism to be Si−Ge interdiffusion.

In situ annealing with TEM observation is very useful for understanding the dynamics of various strain relaxation processes. However, it is challenging to directly observe the nucleation of defects, such as misfit dislocations, within the time frame of a recorded video. To further study other strain relaxation mechanisms, including surface roughening and defect nucleation in core−shell nanowires, postgrowth annealing experiments in hydrogen were performed in the low-pressure CVD nanowire growth chamber. Hydrogen annealing of the SiGe shell promotes Si and Ge surface diffusion,[43,44] and this may create a more roughened sidewall surfaces compared to vacuum anneals in the TEM column. The as-grown core−shell nanowires were dipped in 2% diluted hydrofluoric acid to remove the native oxide prior to their reintroduction into the growth chamber for annealing.

Dislocations and stacking faults were observed when the as-grown nanowires were annealed in hydrogen at 600 °C for 6 min. Under these conditions, Si−Ge interdiffusion is not expected to relax a major fraction of the initial misfit strain in the coherent core−shell NWs. TEM bright-field (BF)/weak-beam dark-field (WBDF) methods were used to image the nucleated dislocation loops after annealing. As circled in Figure 4a,b, dislocations correspond to sharp contrast features that are dark in BF images and are bright in WBDF images. A two-beam condition with a (220) reflection was realized by tilting the wire off the [$\bar{1}$10] zone axis with the nanowire radius direction as the rotational axis. The observed defects were confirmed to be dislocations by the distorted atomic arrangement shown in corresponding high-resolution TEM images. The majority of dislocations have ± $a/2[101]$ or ±$a/2[011]$ Burgers vector inclined 60° from the in-plane [112] direction. These are perfect dislocations with Burgers circuits drawn in Figure 4c, resulting in extra {111} planes that are clearly identified. Because of the high stress concentration at the valleys of the surface undulation, such dislocations are likely to have nucleated close to the roughened surface and then glided along the {111} slip planes through the shell to the Ge-core/SiGe-shell interface. In Figure 4d, a higher magnification image of region 3 clearly shows an intrinsic stacking fault, bounded by two $a/6⟨112⟩$-type Shockley partial dislocations. No $a/3⟨111⟩$-type Frank partial dislocations were observed, in contrast to the results reported previously for Ge-core/Si-shell nanowires that partially relax their misfit strain during shell growth. These

results are, however, consistent with the hypothesis advanced previously for as-grown dislocated Ge core-Si shell nanowires, that surface roughening during postgrowth thermal processes precedes nucleation of defects in core−shell nanowire heterostructures.[12]

To inhibit postgrowth strain relaxation, both surface roughening and interdiffusion need to be suppressed. Formation of a surface oxide may inhibit Si and Ge atom surface diffusion and thus reduce the rate of stress-driven shell roughening for kinetic reasons. The 20 nm Ge-core/2 nm $Si_{0.55}Ge_{0.45}$-shell nanowires, which form roughened surfaces and interfacial defects during hydrogen annealing, were used to test the effect of a thin surface oxide on inhibiting core−shell strain relaxation. The core−shell nanowires were oxidized in atmospheric-pressure UV ozone ambient without intentional heating for 15 min at room temperature. Figure 5 shows that 15
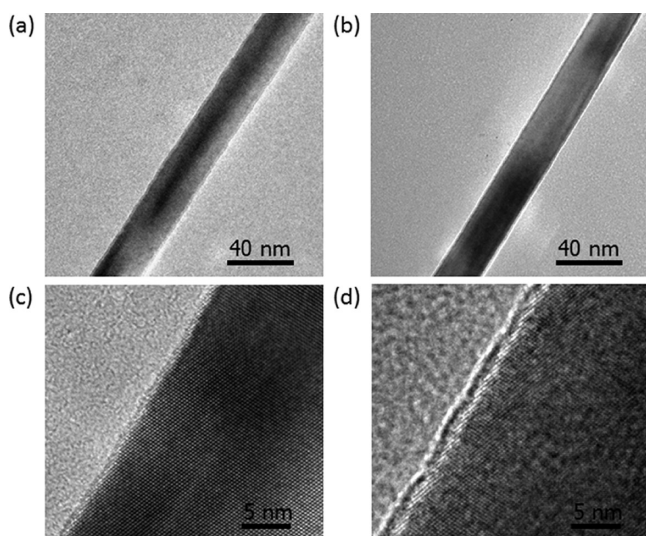
Figure 5. Bright-field images of 20 nm Ge-core/2 nm $Si_{0.55}Ge_{0.45}$ shell nanowires with ∼1 nm UV ozone grown oxide (a) before and (b) after annealing. The oxidized core−shell nanowires were annealed in hydrogen at 600 °C for 6 min. No structural change is apparent when comparing the high-resolution TEM images (c) before and (d) after annealing.

min UV ozone oxidation can form a ∼1 nm oxide shell. Performing the same process on planar $Si_{0.5}Ge_{0.5}$ epitaxial thin films results in a mixture of SiO_2 and GeO_2.[45] After annealing in hydrogen at 600 °C for 6 min, neither surface roughening nor defect formation was observed as shown in Figure 5b. This is in contrast to the results observed after hydrogen annealing of NWs that were not intentionally oxidized.

In summary, we have employed photoluminescence and physical characterization of misfit strain relaxation to understand the surface passivation and thermal stability of highly strained Ge-core/SiGe-shell nanowire heterostructures. Epitaxial SiGe shells of ∼2 nm thickness and ∼55% Si composition were deposited around ⟨111⟩-oriented Ge nanowire cores through inhibition of surface roughening during shell deposition. The high band-edge PL intensity detected from core−shell nanowire arrays, similar to that of bulk Ge (111) substrates, indicates good heteroepitaxial surface passivation of Ge nanowire cores. Strain relaxation mechanisms during postgrowth annealing include Si−Ge interdiffusion, stress-driven surface roughening, and associated dislocation for-

mation. At temperatures above 700 °C, Si−Ge interdiffusion in the nanowire bulk with ∼2.3% core−shell misfit strain was found to be the primary strain relaxation mechanism. Defects, e.g. ⟨110⟩ perfect dislocations and intrinsic stacking faults bounded by ⟨112⟩ Shockley partial dislocations, were observed after roughening of the surfaces of the initially coherent core−shell nanowires during hydrogen anneals at lower temperatures. To inhibit strain relaxation during postgrowth thermal processes at temperatures substantially below those required for significant Si−Ge interdiffusion, a ∼1 nm UV ozone-grown oxide on the core−shell nanowire surfaces was demonstrated to effectively suppress both shell surface roughening and misfit dislocation formation.

■ ASSOCIATED CONTENT

Ⓢ Supporting Information
Experimental details. This material is available free of charge via the Internet at http://pubs.acs.org.

■ AUTHOR INFORMATION

Corresponding Author
*E-mail: pcm1@stanford.edu.

Notes
The authors declare no competing financial interest.

■ ACKNOWLEDGMENTS

■ REFERENCES

(1) Cao, L.; White, J. S.; Park, J.-S.; Schuller, J. A.; Clemens, B. M.; Brongersma, M. L. *Nature Mater.* **2009**, 8, 643−7.
(2) Cao, L.; Park, J.-S.; Fan, P.; Clemens, B.; Brongersma, M. L. *Nano Lett.* **2010**, 10, 1229−33.
(3) Nishi, Y. Study of silicon-silicon dioxide structure by electron spin resonance II. *Jpn. J. Appl. Phys.* **1971**, 10, 52−62.
(4) Nah, J.; Liu, E. S.; Varahramyan, K. M.; Shahrjerdi, D.; Banerjee, S. K.; Tutuc, E. *IEEE Trans. Electron Devices* **2010**, 57, 491−495.
(5) Liang, G.; Xiang, J.; Kharche, N.; Klimeck, G.; Lieber, C. M.; Lundstrom, M. *Nano Lett.* **2007**, 7, 642−6.
(6) Lu, W.; Xiang, J.; Timko, B. P.; Wu, Y.; Lieber, C. M. *Proc. Natl. Acad. Sci. U. S. A.* **2005**, 102, 10046−51.
(7) Zhao, Y.; Smith, J. T.; Appenzeller, J.; Yang, C. *Nano Lett.* **2011**, 11, 1406−11.
(8) Varahramyan, K. M.; Ferrer, D.; Tutuc, E.; Banerjee, S. K. *Appl. Phys. Lett.* **2009**, 95, 033101.
(9) Goldthorpe, I. A.; Marshall, A. F.; McIntyre, P. C. *Nano Lett.* **2009**, 9, 3715−9.
(10) Hellberg, P.-E.; Zhang, S.-L.; Petersson, C. *J. Appl. Phys.* **1997**, 82, 5773.
(11) Prabhakaran, K.; Ogino, T. *Surf. Sci.* **1995**, 325, 263−271.
(12) Goldthorpe, I. A.; Marshall, A. F.; McIntyre, P. C. *Nano Lett.* **2008**, 8, 4081−6.
(13) Lauhon, L. J.; Gudiksen, M. S.; Wang, C. L.; Lieber, C. M. *Nature* **2002**, 420, 57−61.
(14) Xiang, J.; Lu, W.; Hu, Y.; Wu, Y.; Yan, H.; Lieber, C. M. *Nature* **2006**, 441, 489−93.

(15) Adhikari, H.; Marshall, A. F.; Chidsey, C. E. D.; McIntyre, P. C. *Nano Lett.* **2006**, *6*, 318−23.

(16) Guidotti, D.; Hasan, E.; Hovel, H. J.; Albert, M. *Appl. Phys. Lett.* **1987**, *50*, 912.

(17) Lunt, S. R.; Ryba, G. N.; Santangelo, P. G.; Lewis, N. S. *J. Appl. Phys.* **1991**, *70*, 7449.

(18) Steigmeier, E. F.; Morf, R.; Grützmacher, D.; Auderset, H.; Delley, B.; Wessicken, R. *Appl. Phys. Lett.* **1996**, *69*, 4165.

(19) Gurevich, a S.; Kochereshko, V. P.; Bleuse, J.; Mariette, H.; Waag, A.; Akimoto, R. *Nanotechnology* **2011**, *22*, 365707.

(20) Sunamura, H.; Shiraki, Y.; Fukatsu, S. *Appl. Phys. Lett.* **1995**, *66*, 953.

(21) Costa, P. M. F. J.; Datta, R.; Kappers, M. J.; Vickers, M. E.; Humphreys, C. J.; Graham, D. M.; Dawson, P.; Godfrey, M. J.; Thrush, E. J.; Mullins, J. T. *Phys. Status Solidi A* **2006**, *203*, 1729−1732.

(22) Titova, L. V.; Hoang, T. B.; Yarrison-Rice, J. M.; Jackson, H. E.; Kim, Y.; Joyce, H. J.; Gao, Q.; Tan, H. H.; Jagadish, C.; Zhang, X.; Zou, J.; Smith, L. M. *Nano Lett.* **2007**, *7*, 3383−7.

(23) Reitzenstein, S.; Münch, S.; Hofmann, C.; Forchel, A.; Crankshaw, S.; Chuang, L. C.; Moewe, M.; Chang-Hasnain, C. *Appl. Phys. Lett.* **2007**, *91*, 091103.

(24) Kamenev, B. V.; Sharma, V.; Tsybeskov, L.; Kamins, T. I. *Phys. Status Solidi A* **2005**, *202*, 2753−2758.

(25) Klingenstein, W.; Schweizer, H. *Solid-State Electron.* **1978**, *21*, 1371−1374.

(26) Driel, H. M.; van Elci, A.; Bessey, J.; Scully, M. O. *Solid State Commun.* **1976**, *20*, 837−840.

(27) Elkurdi, M.; David, S.; Checoury, X.; Fishman, G.; Boucaud, P.; Kermarrec, O.; Bensahel, D.; Ghyselen, B. *Opt. Commun.* **2008**, *281*, 846−850.

(28) Kawamura, Y.; Huang, K. C. Y.; Thombare, S. V.; Hu, S.; Gunji, M.; Ishikawa, T.; Brongersma, M. L.; Itoh, K. M.; McIntyre, P. C., unpublished work.

(29) Liang, Y.; Nix, W. D.; Griffin, P. B.; Plummer, J. D. *J. Appl. Phys.* **2005**, *97*, 043519−7.

(30) Ozguven, N.; McIntyre, P. C. *Appl. Phys. Lett.* **2008**, *92*, 181907.

(31) Aubertine, D. B.; McIntyre, P. C. *J. Appl. Phys.* **2005**, *97*, 013531.

(32) Meduna, M.; Novák, J.; Bauer, G.; Holý, V.; Falub, C. V.; Tsujino, S.; Grützmacher, D. *Semicond. Sci. Technol.* **2007**, *22*, 447−453.

(33) Xia, G. (Maggie); Canonico, M.; Hoyt, J. L. *Semicond. Sci. Technol.* **2007**, *22*, S55−S58.

(34) Ozkan, C. S.; Nix, W. D.; Gao, H. *Appl. Phys. Lett.* **1997**, *70*, 2247.

(35) Ozkan, C.; Nix, W.; Gao, H. *Mater. Res. Soc. Symp. Proc.* **1998**, *505*, 291−298.

(36) Ozkan, C. S.; Nix, W. D.; Gao, H. *J. Mater. Res.* **2011**, *14*, 3247−3256.

(37) Schmidt, V.; McIntyre, P. C.; Gösele, U. *Phys. Rev. B* **2008**, *77*, 235302.

(38) Ozkan, C. S.; Nix, W. D.; Gao, H. *Appl. Phys. Lett.* **1997**, *70*, 2247.

(39) Gao, H.; Nix, W. D. *Annu. Rev. Mater. Sci.* **1999**, *29*, 173−209.

(40) Shilkrot, L.; Srolovitz, D.; Tersoff, J. *Phys. Rev. B* **2000**, *62*, 8397−8409.

(41) Aziz, M. J. *Appl. Phys. Lett.* **1997**, *70*, 2810.

(42) Aubertine, D. B.; Mander, M. A.; Ozguven, N.; Marshall, A. F.; McIntyre, P. C.; Chu, J. O.; Mooney, P. M. *J. Appl. Phys.* **2002**, *92*, 5027.

(43) Nayfeh, A.; Chui, C. O.; Saraswat, K. C.; Yonehara, T. *Appl. Phys. Lett.* **2004**, *85*, 2815.

(44) Sato, N.; Yonehara, T. *Appl. Phys. Lett.* **1994**, *65*, 1924.

(45) Agarwal, A.; Patterson, J. K.; Greene, J. E.; Rockett, A. *Appl. Phys. Lett.* **1993**, *63*, 518.